Excess Reversing Heat Capacity during Quasi-isothermal Crystallization in Poly(L-lactide) Melt

Takashi SASAKI* and Hikaru SAKURAI*

(received January 30, 2009)

Excess reversing heat capacity C_{ex} of poly(L-lactide) (PLLA) during isothermal crystallization from the melt has been investigated by quasi-isothermal temperature modulated differential scanning calorimetry. Temporal evolution $C_{ex}(t)$ was evaluated on the basis of the two-phase model (crystalline and amorphous phases). At temperatures above 120°C, $C_{ex}(t)$ exhibits a maximum, and the onset of increase in C_{ex} coincides with that of crystallization. On the other hand, at temperatures below 115°C, C_{ex} decreases monotonously from the beginning. These results suggest that the reversible crystallization and melting process is facilitated by the formation of the α phase of PLLA crystal rather than that of the less ordered α' phase. In addition, non-zero excess reversing heat capacity was observed even before the onset of crystallization, indicating the occurrence of reversible crystallization and melting process that is not associated with the crystal growth. On the basis of the three-phase model in which rigid amorphous phase is taken into account, C_{ex} has been revealed to reach a greater value than the initial non-zero value far after the completion of the non-reversible crystallization. Long-term increase in the rigid amorphous fraction was observed after the completion of the crystallization, which suggests formation of secondary crystals.

Key Words : PLLA, crystallization, excess reversing heat capacity, quasi-isothermal TMDSC

1. Introduction

Temperature modulated differential scanning calorimetry (TMDSC) can provide detailed information of thermal events in polymers and has revealed precise behaviors of melting, crystallization, and dynamic glass transition for various polymer systems[1]-[3]. It has been demonstrated by TMDSC that reversible crystallization and melting (RCM) process exists in addition to non-reversible crystallization governed by the nucleation and growth mechanism for various semicrystalline polymers such as polyethylene[4]-[7], poly(ethylene oxide)[4],[5],[8], poly(ethylene terephthalate)[4],[9],[10], poly(ε-caprolactone)[4], ethylene-octene copolymers[6], ethylene-styrene copolymers[11], isotactic and syndiotactic polypropylenes[4],[6], etc. In these cases, apparent reversing heat capacity is greater than the thermodynamic (equilibrium) heat capacity of the material even after the crystallization has ceased. The RCM process essentially occurs with no entropy production, and this is not incorporated in the crystal growth associated with the irreversible nucleation process. There must be some regions where the RCM process occurs in a local equilibrium between crystalline and amorphous states. However, the location of the RCM region is not clear. They might be in the interfacial region between the crystalline and amorphous phases, either on the fold surface or on the lateral surface of lamella crystallites[4],[9]. Alternatively, they might be separated from the primary lamellae, being independent of their growth. The RCM mechanism seems to depend on various factors especially on the material and thermal history.

Poly(L-lactide) (PLLA) is one of the most popular polymers that can be used as a biodegradable material, and various thermal properties of this polymer have been extensively studied so far. TMDSC has been utilized to investigate the heat capacity and dynamics around the glass transition for PLLA[12]-[14]. Crystallization mechanism of PLLA is also an important subject, because crystallinity affects its mechanical and thermal properties significantly. However, the crystallization behaviors of PLLA have been revealed to be rather complicated[15]. For example, a discontinuous change in crystallization behaviors has been reported to occur at 113°C[16]. Also, PLLA freeze-dried from a very dilute solution exhibits

*Materials Science and Engineering Course, Graduate School of Engineering

a cold crystallization signal at a temperature 20 K lower than the usual bulk PLLA[17],[18]. In addition, an issue concerning different crystal structures of PLLA has been raised recently. Three different crystalline modifications are known for PLLA, *i.e.*, the α, β, and γ structures[19]-[22], but a less ordered structure than the α modification (referred to as the α' structure) has been found to occur at low crystallization temperatures[23],[24]. The α' phase can be converted to the α phase on heating.

The existence of excess reversing heat capacity in PLLA has been demonstrated[25], but more precise data, especially temporal change of the excess reversing heat capacity during crystallization has not been reported so far. The RCM process probably plays an important role in crystallization of PLLA, and therefore, it is intriguing to elucidate its origin and mechanism in detail.

In this work, we investigate the excess reversing heat capacity for PLLA during melt crystallization by the quasi-isothermal TMDSC, and attempt to interpret the results in terms of crystallinity, crystal structure, and the heterogeneous rigid amorphous phase. The excess reversing heat capacity C_{ex} can be obtained from the quasi-isothermal TMDSC measurements as $C_{ex} = C_{ap} - C_0$, where C_{ap} is the apparent reversing heat capacity, and C_0 is the thermodynamic heat capacity due to vibrational degree of freedom and to additional degree of freedom of the liquid phase. C_{ap} must be reversing heat capacity in the sense that it is reversible within the experimental amplitude and frequency of modulation. The excess heat capacity thus obtained has been assumed to reflect the RCM process. In this study, we have measured time evolutions of both C_{cx} and crystallinity simultaneously from a quasi-isothermal TMDSC scan. Our method provides reliable information about the RCM process, which allows us to discuss precise mechanism for the melt crystallization of PLLA.

2. Experimental

PLLA was supplied by Mitsui Chemicals Co. (M_w = 210 kg mol^{-1}, 98% L units). Non-crystallizable polylactide copolymer of D and L units (PDLLA) was purchased from Aldrich, which was used to determine the thermodynamic heat capacity in the liquid state. To remove volatile impurities the polymers were freeze-dried from a 7.0wt% 1,4-dioxane solution, and was further dried under vacuum at 46°C for 24 h. For the calorimetry measurements we used a DSC calorimeter Perkin Elmer Pyris Diamond. As a cooling system, either an ice-water bath or an ethylene glycol-propylene glycol bath (kept at –30 °C) was used. The temperature and heat flow were calibrated by an indium standard. All measurements were performed in a nitrogen atmosphere. Typical sample size ranged from 6 to 10 mg.

Time evolution of the excess reversing heat capacity during melt crystallization was obtained by the quasi-isothermal TMDSC. Measurement was repeated several times for different specimens to check the reproducibility. PLLA sample was first heated at 185°C or 210°C for 2 min, and then, it was quenched to T_c (crystallization temperature), and then, a modulation with a saw-tooth profile was applied[26], of which the period and amplitude were 60 s and 0.5 K, respectively. T_c ranged from 90 to 130°C. We confirmed that the Lissajous figures (heat flow vs. temperature) showed no apparent distortion throughout the scanning period, thus the present condition of temperature modulation satisfied the 'reversing condition' that the thermal response is recovered in one period of the modulation.

The present quasi-isothermal condition with the small amplitude of modulation is assumed to allow PLLA to undergo isothermal crystallization from the melt. From the observed heat flow data, the apparent reversing heat capacity (at constant pressure) was evaluated as

$$C_{ap}(t) = A_{HF} \cdot K / (A_T \omega) \qquad (1)$$

where A_{HF} and A_T are the first harmonic components of the Fourier transformation of the observed heat flow and sample temperature, respectively, and ω is the modulation frequency. K is a correction constant, which includes a time constant of heat conduction τ, and modulation frequency ω as[11],[26]

$$K \propto \sqrt{1+\tau^2 \omega^2} \qquad (2)$$

We evaluated K by extrapolation of a reference sample data to zero frequency, and the absolute value of C_{ap} was further corrected using a sapphire standard.

The excess reversing heat capacity was evaluated by

$$C_{ex}(t) = C_{ap}(t) - C_0(t) \qquad (3)$$

where $C_0(t)$ is the thermodynamic heat capacity for the semi-crystalline PLLA, which includes no contributions from reversible latent heat effects. During the quasi-isothermal crystallization, $C_0(t)$ changes with time as the crystallinity increases. We evaluated $C_0(t)$ based on the two-phase (amorphous liquid and crystal) model as

$$C_0(t) = X_c(t)\, C_s + (1 - X_c(t))\, C_l \qquad (4)$$

where C_s and C_l are the heat capacities of the solid (crystalline and/or glassy) and liquid states, respectively, and $X_c(t)$ is the temporal evolution of crystallinity (degree of crystallization).

To evaluate the heat capacities C_s and C_l, we performed measurements of the step-scan heating mode of DSC[17]. The repeating unit of the step-scan profile consisted of a heating step of 2 K at a rate of 5 K min^{-1} followed by an isotherm step which ended after 10 consecutive points of heat flow fell within ±0.01 mW. C_s was obtained from the heat capacity data for PLLA in a temperature range of 0 – 45°C, and extrapolation to higher temperatures was executed. As for C_l, we used the step-scan data for PDLLA to avoid the effect of crystallization during the scan. The obtained heat capacity data were further corrected by using a calibration with respect to a sapphire standard. The step-scan measurements for C_s and C_l were repeated more than 10 times for different specimens and their averaged traces were analyzed.

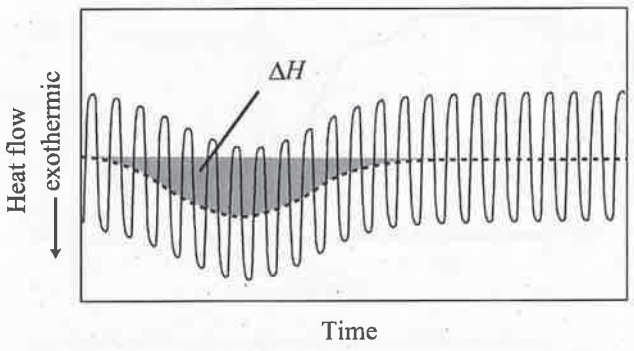

Fig. 1 Typical heat flow curve observed during quasi-isothermal TMDSC scan. The dotted curve indicates baseline trace of the heat flow. The heat of crystallization was evaluated as the indicated area.

Time evolution of crystallinity $X_c(t)$ was evaluated from the baseline drift of the modulated heat flow as depicted in Fig. 1. In addition, to confirm the value of ultimate crystallinity $X_c(\infty)$, a conventional DSC scan from T_c to 185°C was performed at 10 K min^{-1} immediately after the quasi-isothermal TMDSC measurement. From the observed endotherm, calorimetric crystallinity was evaluated. In the evaluation of the crystallinity, we used a literature value of the enthalpy of fusion for PLLA as 90.9 J g^{-1} K^{-1} [27].

During the crystallization of PLLA, rigid amorphous phase that has lower mobilities due to the constraint imposed by the crystalline lamellae may be formed[28],[29]. Such rigid amorphous phase may play an important role in the melt crystallization, thus we also evaluated its amount and tried to correct the C_{ex} data with respect to this contribution. After the completion of the melt crystallization the sample was quenched to 28°C, and then a heating step-scan was executed to evaluate the heat capacity change ΔC_p at the glass transition temperature T_g. The step-scan conditions were the same as mentioned above. The ultimate rigid amorphous fraction $X_{RA}(\infty)$ was obtained by

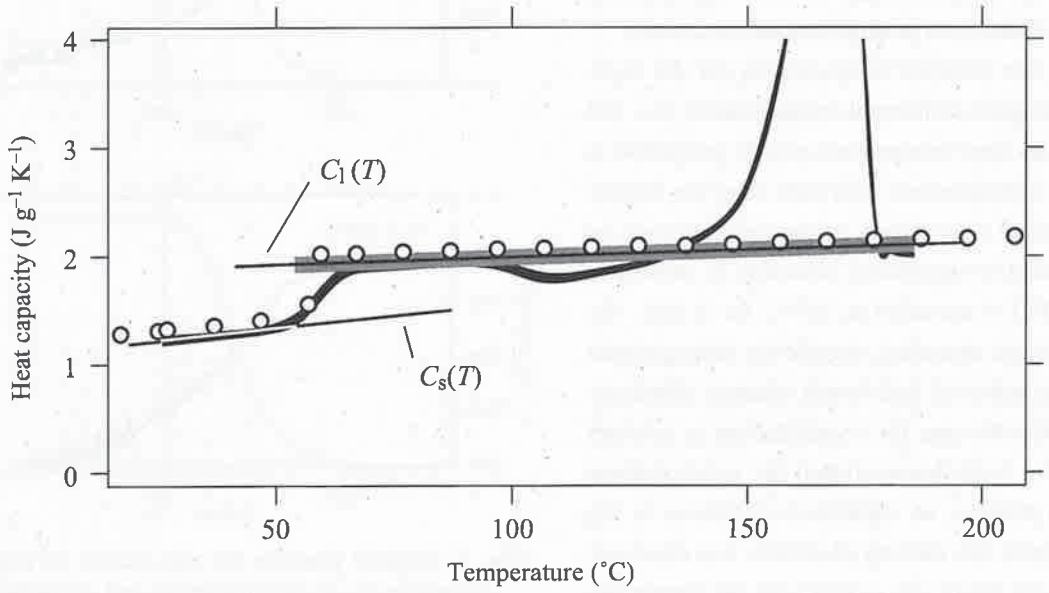

Fig. 2 Thermodynamic heat capacities for PLLA and PDLLA obtained by the step-scan mode of DSC. The thick solid curve indicates the heat capacity for PLLA quenched from the melt, and the gray thick line indicates that for PDLLA (presented only for the data above T_g). The open circles indicate the literature values of Ref. [27]. The thin lines represent fitted lines for $C_s(T)$ and $C_l(T)$ obtained by the linear regression analysis; the expressions are given in the text.

$$X_{RA}(\infty) = 1 - X_c(\infty) - \Delta C_p / \Delta C_p^0 \quad (5)$$

where ΔC_p^0 is the heat capacity change at T_g for a complete amorphous material. ΔC_p^0 was evaluated as a difference between C_l and C_s at the observed T_g. The experimental relations for C_l and C_s are presented in the following section. Time evolution of the rigid amorphous fraction $X_{RA}(t)$ was also measured by interrupting the quasi-isothermal crystallization at several different times by quenching the sample to 28°C, followed by a heating step-scan.

FT-IR measurements in the attenuated total reflection mode were performed for the crystallized PLLA to investigate their crystal structure by using a Nicolet Nexus 870 infrared Raman spectrometer.

3. Results

Figure 2 shows the thermodynamic heat capacities C_s and C_l which were obtained by the step-scan heating measurements. Linear regression analysis exhibited good fits to the data which yielded $C_s(T)$ / (J g^{-1} K^{-1}) = 1.1202 + 0.0042354 (T / °C), and $C_l(T)$ / (J g^{-1} K^{-1}) = 1.8493 + 0.0014012 (T / °C), where T is the sample temperature. The thin solid lines in Fig. 2 show the above fitted relations. We used these relations to calculate $C_0(t)$ according to Eq (4). The open circles indicate reported heat capacities obtained by Pyda et al[27]. Slight deviations are seen from the reported data, which may be due to the difference in material (molecular weight, purity, etc.), or to the differences in experimental conditions.

We chose two different temperatures for the melting prior to the quasi-isothermal crystallization, *i.e.*, 185 and 210°C. The latter temperature may be preferable to achieve more homogeneous melt state than the former. However, thermal degradation of the polymer may be serious: we found a significant reduction in molecular weight for a PLLA annealed at 210°C for 2 min. By even such a severe annealing, completely homogeneous state can not be achieved, and certain memory effects exist. This is even the case for crystallization in polymer solutions as we have demonstrated for poly(ethylene oxide)[30]. In practice, no significant difference in C_{ex} between the above two melting conditions was observed. Thus, we present below the results with the former annealing (at 185°C for 2 min) for which less degradation of PLLA is expected.

Figure 3 shows time-dependent excess reversing heat capacity $C_{ex}(t)$ obtained at different crystallization temperatures. Time evolutions of the crystallinity obtained simultaneously are also plotted. We see that at temperatures lower than 115°C, $C_{ex}(t)$ decreases monotonously from the beginning, while at higher temperatures

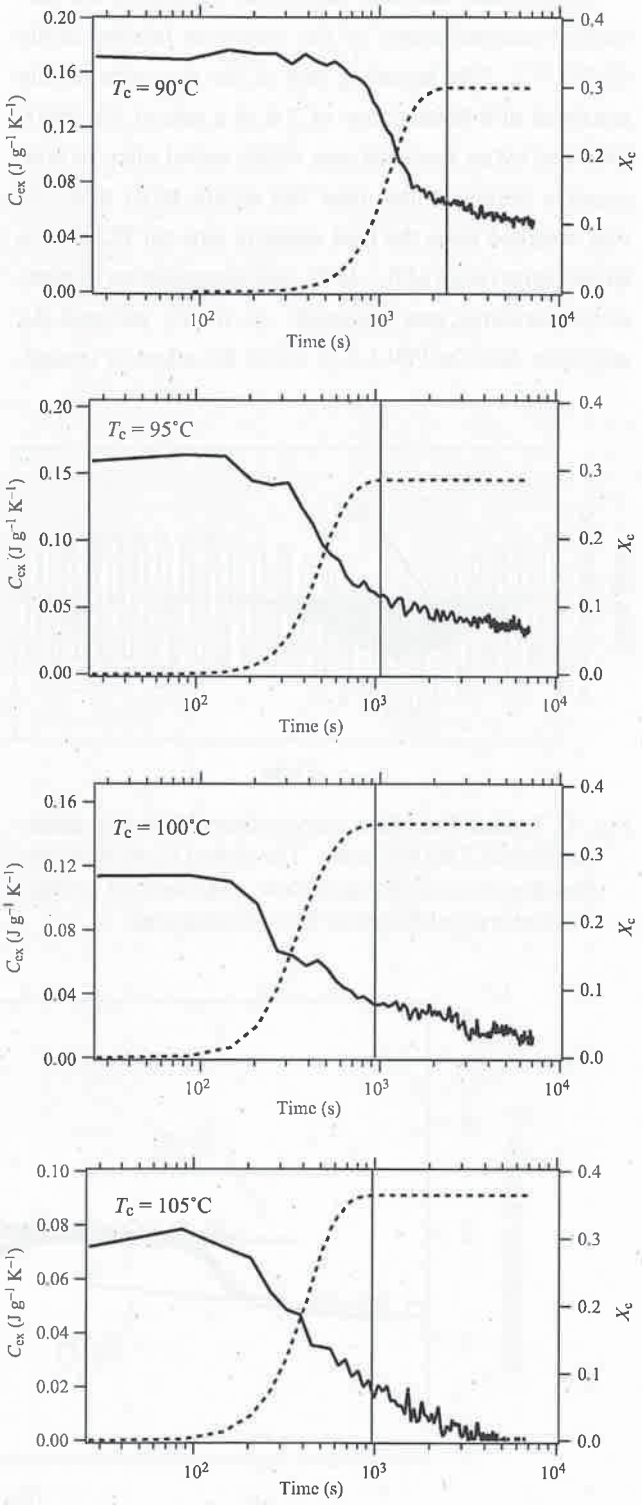

Fig. 3 Typical profiles for the excess reversing heat capacities $C_{ex}(t)$ (solid curves) and crystallinity $X_c(t)$ (dotted curves) obtained by the quasi-isothermal TMDSC measurements. Here, $C_{ex}(t)$ was evaluated according to the two-phase model. The vertical lines indicate the time when the non-reversible crystallization has almost ceased.

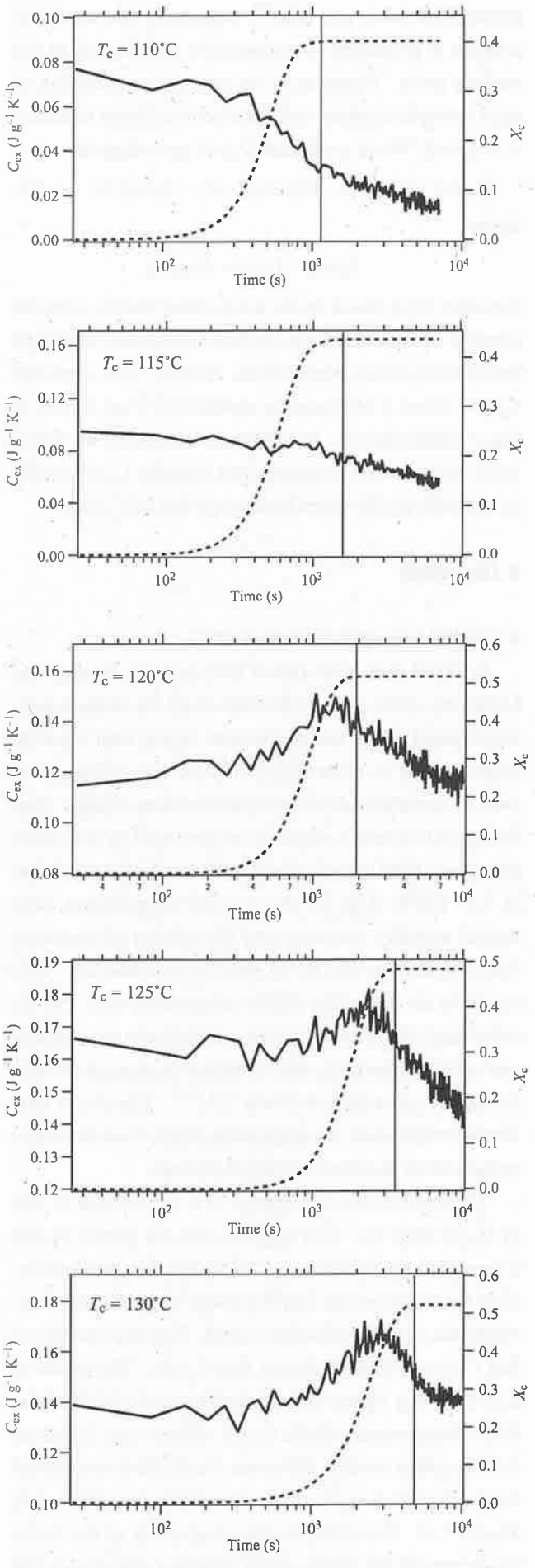

Fig. 3 (*Continued from the preceding page.*)

above 120°C C_{ex} exhibits a maximum. The maximum position (time) shifts to later times as the crystallization temperature is raised. It is noted that the decrease in C_{ex} continues even after the completion of the non-reversible crystallization as shown in Fig. 3 (the vertical lines show the endpoint of crystallization). This is the case for all the temperatures investigated (90 – 130°C). The ultimate crystallinity $X_c(\infty)$ obtained at sufficiently long time (> 3 h) increases with increasing temperature as shown in Table 1. This means that the crystallizable fraction in the material increases with increasing T_c, due to increase in segmental mobility.

The overall crystallization rate R was estimated with a reciprocal of the half-time for reaching the final crystallinity, *i.e.*, $R = 1/t_{0.5}$. The results are shown in Table 1. A maximum is seen at around 100 – 110°C. However, the discontinuity that has been reported to occur at 110 – 120 °C[16],[31] is not obviously seen. The reason for this is not clear, but if the discontinuity arises from the regime II - III transition[32], it would be reflected more clearly in the linear growth rate rather than the overall crystallization rate.

The data of C_{ex} in Fig. 3 is probably affected by the rigid amorphous fraction X_{RA}, because they were obtained on the basis of the two-phase model in which the contribution from the rigid amorphous phase was not taken into account. Table 1 shows ultimate values of $X_{RA}(\infty)$ obtained at sufficiently long time (> 3 h). We see that $X_{RA}(\infty)$ decreases with increasing temperature. The rigid amorphous phase may be rather heterogeneous having wide variety of mobilities, and the amorphous phase in semicrystalline PLLA has a distribution of relaxation times broader than that of the amorphous phase in non-crystalline PLLA. At elevated temperatures, only the amorphous portions with lower mobilities remain glassy

Table 1 Ultimate crystallinity, overall crystallization rate, and ultimate rigid amorphous fraction

T_c (°C)	$X_c(\infty)$	R (10^{-3} s^{-1})	$X_{RA}(\infty)$
90	0.29 ± 0.01	0.89 ± 0.05	0.35 ± 0.01
95	0.31 ± 0.02	1.32 ± 0.18	0.32 ± 0.01
100	0.34 ± 0.02	1.69 ± 0.46	0.29 ± 0.02
105	0.37 ± 0.01	1.56 ± 0.04	0.27 ± 0.01
110	0.40 ± 0.01	1.67 ± 0.29	0.27 ± 0.01
115	0.43 ± 0.01	1.35 ± 0.09	0.26 ± 0.02
120	0.46 ± 0.03	1.11 ± 0.07	0.22 ± 0.02
125	0.50 ± 0.04	0.66 ± 0.09	0.17 ± 0.02
130	0.52 ± 0.04	0.51 ± 0.09	0.18 ± 0.03

on the time scale of the DSC measurement. This results in smaller X_{RA}'s at higher temperatures. Arnoult et al. obtained a value of $X_{RA}(\infty)$ smaller than the present results[29]. The reason for this discrepancy is not clear, but may be partially due to the difference in crystallization condition.

Figure 4 shows time evolutions of the rigid amorphous fraction $X_{RA}(t)$ at T_c = 90°C and 130°C in the time period after the completion of crystallization. Slightly increasing profiles with respect to time are observed. This suggests that certain structural change occurs even after the crystallization has ceased, and this may be connected with the apparent log-term decrease in C_{ex} shown in Fig. 3.

We found that the ultimate excess heat capacity $C_{ex}(\infty)$ based on the two-phase model tends to increase with increasing T_c. This tendency has been generally

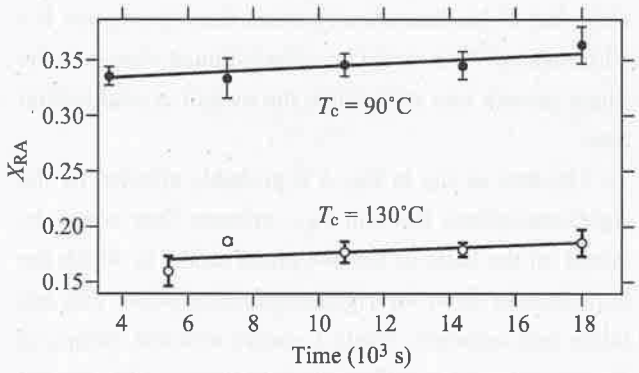

Fig. 4 Rigid amorphous fraction $X_{RA}(t)$ vs. time in the period after the completion of the crystallization. The solid lines indicate results of linear regression analysis.

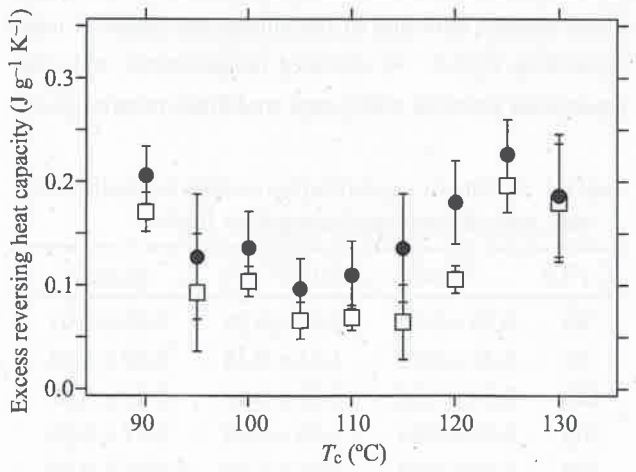

Fig. 5 Excess reversing heat capacities with respect to the crystallization temperature T_c. Filled circles indicate $C_{ex}(\infty)$ values corrected for the rigid amorphous fraction according to Eq (6), and open squares indicate the initial values $C_{ex}(0)$.

reported for other polymers[4], suggesting that the RCM process is promoted as temperature approaches to the melting point. However, if we take the contribution of rigid amorphous phase into account, a different tendency is obtained. We re-evaluated $C_{ex}(\infty)$ according to

$$C_{cx}(\infty) = C_{ap}(\infty) - X_s(\infty)\, C_s - (1 - X_s(\infty))\, C_l \qquad (6)$$

where

$$X_s(\infty) = X_c(\infty) + X_{RA}(\infty)$$

Equation (6) is based on the assumption that the material consists of the crystalline, mobile amorphous, and rigid amorphous phases (three-phase model). The corrected $C_{ex}(\infty)$ shows a minimum at around 105°C as shown in Fig. 5 (filled circles). In addition, we note that the initial value of the excess reversing heat capacity $C_{ex}(0)$ exhibits a similar profile (open squares) to that of $C_{ex}(\infty)$.

4. Discussion

4.1 Initial and ultimate values of C_{ex}

In Fig. 3, non-zero excess heat capacity is observed before the onset of crystallization at all the temperatures investigated. This initial non-zero excess heat capacity might be due to reversible formation and melting process of unstable nuclei (with dimensions smaller than the critical nucleus), which is not governed by activation processes. The initial value $C_{cx}(0)$ exhibits a minimum at T_c = 105°C (Fig. 5). At elevated temperatures, segmental mobility increases and the number of segments that can undergo the RCM process is enhanced. This results in the rise at the higher temperature end. On the other hand, the origin of the rise at the lower temperature end might be partially due to higher nucleation density during the quenching to lower T_c's[33]. The nuclei thus formed might make the amorphous phase more heterogeneous, which facilitates the RCM process.

The profile of $C_{ex}(\infty)$ against T_c is very similar to that of $C_{ex}(0)$ (Fig. 5). This suggests that the former profile is governed by the latter, that is, the RCM region responsible for the non-zero $C_{ex}(0)$ persists long after the non-reversible crystallization has ceased. Figure 5 also shows that $C_{ex}(\infty)$ is slightly greater than $C_{ex}(0)$. The values of $C_{ex}(\infty)$ in this figure were evaluated on the basis of the three-phase model, while $C_{ex}(0)$ values were based on the two-phase model. However, $C_{ex}(0)$ does not depend on the model, because it is reasonable to assume that $X_{RA}(0) = 0$. Therefore, on the assumption of the three-phase model, the above result indicates that the excess

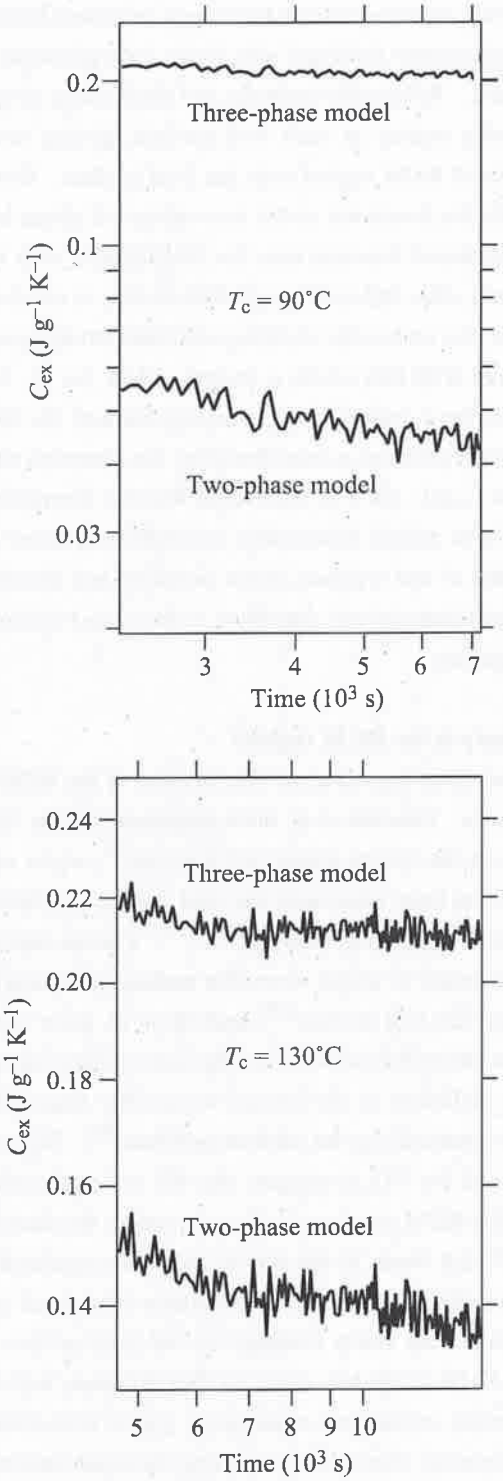

Fig. 6 Comparison of the excess reversing heat capacities in the late period based on the two- and three-phase models.

reversing heat capacity increases after the non-reversible crystallization. This means that the RCM region is greater in semi-crystalline PLLA than in complete amorphous PLLA, and that the RCM process still remains after the non-reversible crystallization has ceased.

4.2 Contribution of the rigid amorphous phase

It is reasonably assumed that $X_{RA}(t)$ increases in accord with the increase in $X_c(t)$ during crystallization. In addition, $X_{RA}(t)$ slightly increases even after the completion of the crystallization as shown in Fig. 4. Unfortunately, we could not obtain detailed time evolution data of X_{RA} because of experimental difficulty, and therefore, we could not obtain profiles of $C_{ex}(t)$ based on the three-phase model according to Eq (6). (It would be more difficult to obtain precise $X_{RA}(t)$ data during the crystallization than in the period of constant crystallinity.) Here we present rough evaluation of $C_{ex}(t)$ on the basis of the three-phase model using the data in Fig. 4 only in the later period after the completion of the crystallization. The results are shown in Fig. 6, showing that C_{ex} of the three-phase model is nearly independent of time. In Fig. 3, C_{ex} decreases even after the completion of the crystallization, but this is now corrected by the three-phase model. The constancy of C_{ex} in spite of X_{RA} indicates that the RCM region is not reduced by the increased portion of rigid amorphous phase. This suggests that the location of the rigid amorphous region is separated from the RCM region.

However, one could hardly conceive that the rigid amorphous region develops slightly even after the completion of the crystallization, because it is generally considered that the formation of rigid amorphous phase is associated with crystal growth. This log-term increase in X_{RA} might be related to the secondary crystallization. Some semi-crystalline polymers that contain non-crystallizable segments such as copolymers generally exhibit multiple melting behaviors. This has often been attributed to the secondary crystallization[11],[34]-[37], *i.e.*, to subsidiary crystallization that is associated with formation of unstable bundle-like crystallites with fewer chain foldings than in the primary lamellar crystallites. Isothermally crystallized PLLA exhibits a double-melting behavior when crystallized at lower temperatures[38], but this has been attributed to melting-recrystallization process or to the transition from the α' to α phase. Aside from this, the secondary crystallization associated with the formation of very unstable crystallites or bundle-like nuclei in the liquid phase might occur even after the completion of the lamellar growth, which leads to slight decrease of the thermodynamic heat capacity C_0, resulting in the increase of apparent X_{RA}.

4.3 Time evolution profile of C_{ex}

From the above discussion based on the three-phase model, we infer that the profile of corrected $C_{ex}(t)$ could

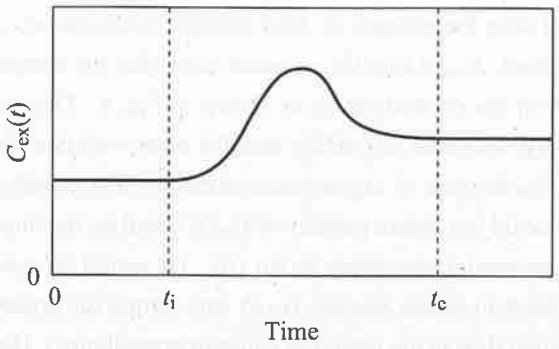

Fig. 7. Schematic representation of the assumed profile of $C_{ex}(t)$ based on the three-phase model. The onset and endpoint of the non-reversible crystallization is indicated as t_i and t_e, respectively.

be depicted as in Fig. 7. The maximum shown in Fig. 3 is retained if we employ the three-phase model[1]. The origin of the maximum may be explained as follows. In the early stage of crystallization, the RCM region increases as the interfacial region grows with crystallization, which gives rise to the additional increase from the non-zero $C_{ex}(0)$. In the late stage, the surface-to-volume ratio of crystallites decreases as the crystals grow, and impingements of crystallites (spherulites) further consume the mobile interfacial region, therefore, C_{ex} decreases. The onset of the increase in C_{ex} coincides with that in X_c. C_{ex} becomes constant after the completion of the crystallization as evidenced by Fig. 6.

For isothermal crystallization of PLLA, it has been reported that at low temperatures below 120°C, the less ordered α' phase occurs[22]. This loose structure may be hexagonal packing, and can be characterized by wide-angle X-ray diffraction and FT-IR spectroscopy[23],[24]. It has also been reported that the α' and α modifications are exclusively obtained when $T_c \leq 90$°C and $T_c \geq 120$°C, respectively[24]. In the intermediate temperature range, an intermediate crystalline structure between the α' and α phases is formed which may be either a mixture of the two phases, or an intermediately ordered phase[24]. For our PLLA samples, we confirmed that qualitatively the same temperature dependence of the crystalline structure as the above reported results by FT-IR spectroscopy: absorption bands at 1749 and 1382 cm^{-1} which are characteristic to the α modification[23] were reduced as T_c decreases from 120°C to 90°C, and at 90°C, they were not discernible.

Formation of the α structure may lead to fold surface of primary lamellae where short loops and sharp foldings (adjacent reentry foldings) with fewer entanglements are dominant. Reversible melting and thickening process preferably occurs at such fold surface, giving rise to increase of RCM region near the fold surface. On the contrary, the formation of the less ordered α' phase leads to a disordered structure near the fold surface, with long loops and cilia, and such rough fold surface is not favorable for the reversible melting and thickening process compared with that of the α crystal. Thus, for T_c 120° C where the α crystals are exclusively formed, the RCM process is enhanced as manifested by the observed maximum in $C_{ex}(t)$. As it is considered that the formation of the α' form occurs kinetically, reversible transition between the α' and α phases is not possible, and therefore, such transition can not contribute to the excess reversing heat capacity.

4.4 Where is the RCM region?

It has been argued about the location of the RCM region so far. Okazaki et al. have proposed that the RCM occurs on the lateral surface of lamellae[9], while other researchers have advocated the fold surface mechanism (reversible thickening model)[4],[11],[39]. Fischer has proposed a model in which reversible melting is assumed to occur on the fold surface[40], and Hu et al. have shown that the reversible process on the fold surface through sliding diffusion in the crystal is possibly responsible for the observed C_{ex} for various polymers[4]. The present results for PLLA suggest that the ordered α phase favors the RCM process. In the α structure, the direction of the PLLA chain in the crystal has to be regulated[19], and such directional order is favorably associated with tight loops and sharp foldings on the fold surface. A recent NMR study has revealed that diffusion between the lamellar crystal and amorphous region is facilitated by preferential chain diffusion along the chain backbone rather than by isotropic diffusion[41]. The short loops and sharp foldings associated with the α structure are effective for such preferential diffusion that is connected with the sliding diffusion in the crystal. We thus conclude that the RCM region that is responsible for the maximum in $C_{ex}(t)$ at the higher T_c's is likely located at the fold surface. Another type of RCM region exists as evidenced by the non-zero excess heat capacity observed before the onset of the non-reversible crystallization as we mentioned in the previous section. This type of RCM may be located in the amorphous phase separated from the

1) The rising profile in $C_{ex}(t)$ is expected to be emphasized by the three-phase model provided that X_{RA} increases with time.

primary lamellae.

5. Conclusions

The present study has revealed that on the basis of the two-phase model the excess reversing heat capacity C_{ex} in PLLA during quasi-isothermal crystallization from the melt exhibits different evolutions depending on T_c. C_{ex} has been revealed to exhibit a maximum at temperatures above 120°C, and this may be attributed to the formation of the ordered α phases. The α structure may lead to tight loops on the fold surface of lamellae, which promotes the RCM process in the interfacial region, and therefore, C_{ex} tends to increase as the α structure develops for $T_c \geq 120$°C. Based on the above consideration, we infer that the RCM region that is responsible for the additionally increased C_{cx} manifested by the maximum is mainly located on the fold surface.

The non-zero excess heat capacity observed in the early time period suggests that the RCM process also occurs in the amorphous phase independent of the primary lamellae. Long-term increase in X_{RA} was observed, which might be attributed to the formation of unstable secondary crystals. Based on the three-phase model in which the rigid amorphous phase is taken into account, C_{ex} is revealed to reach an ultimate value slightly greater than $C_{ex}(0)$ at all the temperatures investigated, indicating that the RCM region is extended by crystal growth. $C_{ex}(t)$ profile exhibits a maximum at temperatures above 120°C, which is expected to become prominent if we employ the three-phase model. Such additional increase in C_{ex} is characteristic to the α structure of PLLA. Precise evaluation of $X_{RA}(t)$ during the period of crystal growth is needed to elucidate the entire profile of $C_{ex}(t)$ on the basis of the three-phase model.

References

[1] Schawe, J. E. K. *Thermochim. Acta* **1995**, *261*, 183.

[2] Schawe, J. E. K. *Thermochim. Acta* **1997**, *304/305*, 111.

[3] Wuderlich, B. *Progr. Polym. Sci.* **2003**, *28*, 383 and references therein.

[4] Hu, W.; Albrecht, T.; Strobl, G. *Macromolecules* **1999**, *32*, 7548.

[5] Albrecht, T.; Armbruster, S.; Keller, S.; Strobl, G. *Macromolecules* **2001**, *34*, 8456.

[6] Androsch, R.; Wunderlich, B. *J. Polym. Sci. Part B: Polym. Phys.* **2003**, *41*, 2039.

[7] Androsch, R.; Wunderlich, B. *J. Polym. Sci. Part B: Polym. Phys.* **2003**, *41*, 2157.

[8] Ishikiriyama, K.; Wunderlich, B. *Macromolecules* **1997**, *30*, 4126.

[9] Okazaki, I.; Wunderlich, B. *Macromolecules* **1997**, *30*, 1758.

[10] Okazaki, I.; Wunderlich, B. *Macromol. Rapid Comun.* **1997**, *18*, 313.

[11] Huang, Z.; Marand, H.; Cheung, W. Y.; Guest, M. *Macromolecules* **2004**, *37*, 9922.

[12] Pyda, M.; Wunderlich, B. *Macromolecules* **2005**, *38*, 10472.

[13] Mano, J. F.; Gómez Ribelles, J. L.; Alves, N. M.; Salmerón Sánchez, M. *Polymer* **2005**, *46*, 8258.

[14] Wang, Y.; Gómez Ribelles, J. L.; Salmerón Sánchez, M.; Mano, J. F. *Macromolecules* **2005**, *38*, 4712.

[15] Cho, T. Y.; Strobl, G. *Polymer* **2006**, *47*, 1036.

[16] Yasuniwa, M.; Tsubakihara, S.; Iura, K.; Ono, Y.; Dan, Y.; Takahashi, K. *Polymer* **2006**, *47*, 7554.

[17] Sasaki, T.; Yamauchi, N.; Irie, S.; Sakurai, K. *J. Polym. Sci. Part B: Polym. Phys.* **2005**, *43*, 115.

[18] Sasaki, T.; Tabata, N.; Sakurai, K. to be submitted.

[19] Alemán, C.; Lotz, B.; Puiggali, J. *Macromolecules* **2001**, *34*, 4795.

[20] Kobayashi, J.; Asahi, T.; Ichiki, M.; Okikawa, A.; Suzuki, H.; Watanabe, T.; Fukuda, E.; Shikinami, Y. *J. Appl. Phys.* **1995**, *77*, 2957.

[21] Cartier, L.; Okihara, T.; Ikada, Y.; Tsuji, H.; Puiggali, J.; Lotz, B. *Polymer* **2000**, *41*, 8909.

[22] Puiggali, J.; Ikada, Y.; Tsuji, H.; Cartier, L.; Okihara, T.; Lotz, B. *Polymer* **2000**, *41*, 8921.

[23] Zhang, J.; Duan, Y.; Sato, H.; Tsuji, H.; Noda, I.; Yan, S.; Ozaki, Y. *Macromolecules* **2005**, *38*, 8012.

[24] Kawai, T.; Rahman, N.; Matsuba, G.; Nishida, K.; Kanaya, T.; Nakano, M.; Okamoto, H.; Kawada, J.; Usuki, A.; Honma, N.; Nakajima, K.; Matsuda, M. *Macromolecules* **2007**, *40*, 9463.

[25] Salmerón Sánchez, M.; Gómez Ribelles, J. L.; Hernández Sánchez, F.; Mano, J. F. *Thermochim. Acta* **2005**, *430*, 201.

[26] Androsch, R.; Moon, I.; Kreitmeier, S.; Wunderlich, B. *Thermochim. Acta* **2000**, *357/358*, 267.

[27] Pyda, M.; Bopp, R. C.; Wunderlich, B. *J. Chem. Thermodyn.* **2004**, *36*, 731.

[28] Brás, A. R.; Viciosa, M. T.; Wang, Y.; Dionísio, M.; Mano, J. F. *Macromolecules* **2006**, *39*, 6513.

[29] Arnoult, M.; Dargent, E.; Mano, J. F. *Polymer* **2007**, *48*, 1012.

[30] Sasaki, T.; Yamamoto, Y.; Takahashi, T. *Polym. J.* **1998**, *30*, 868.

[31] Di Lorenzo, M. L. *Eur. Polym. J.* **2005**, *41*, 569.

[32] Tsuji, H.; Tezuka, Y.; Saha, S. K.; Suzuki, M.; Itsuno, S. *Polymer* **2005**, *46*, 4917.

[33] Salmerón Sánchez, M.; Mathot, V. B. F.; Poel, G. V.; Gómez Ribelles, J. L. *Macromolecules* **2007**, *40*, 7989.

[34] Androsch, R.; Wunderlich, B. *Macromolecules* **1999**, *32*, 7238.

[35] Alizadeh, A.; Richardson, L.; Xu, J.; McCartney, S.; Marand, H.; Cheung, Y. W.; Chum, S. *Macromolecules* **1999**, *32*, 6221.

[36] Sohn, S.; Alizadeh, A.; Marand, H. *Polymer* **2000**, *41*, 8879.

[37] Sasaki, T.; Sunago, H.; Hoshikawa, T. *Polym. Eng. Sci.* **2003**, *43*, 629.

[38] Yasuniwa, M.; Iura, K.; Dan, Y. *Polymer* **2007**, *48*, 5398.

[39] Goderis, B.; Reynaers, H.; Scherrenberg, R.; Mathot, V. B. F.; Koch, M. H. J. *Macromolecules* **2001**, *34*, 1779.

[40] Fischer, E. W. *Kolloid Z. Z. Polym.* **1967**, *218*, 97.

[41] Yao, Y.-F.; Graf, R.; Spiess, H. W.; Rastogi, S. *Macromolecules* **2008**, *41*, 2514.